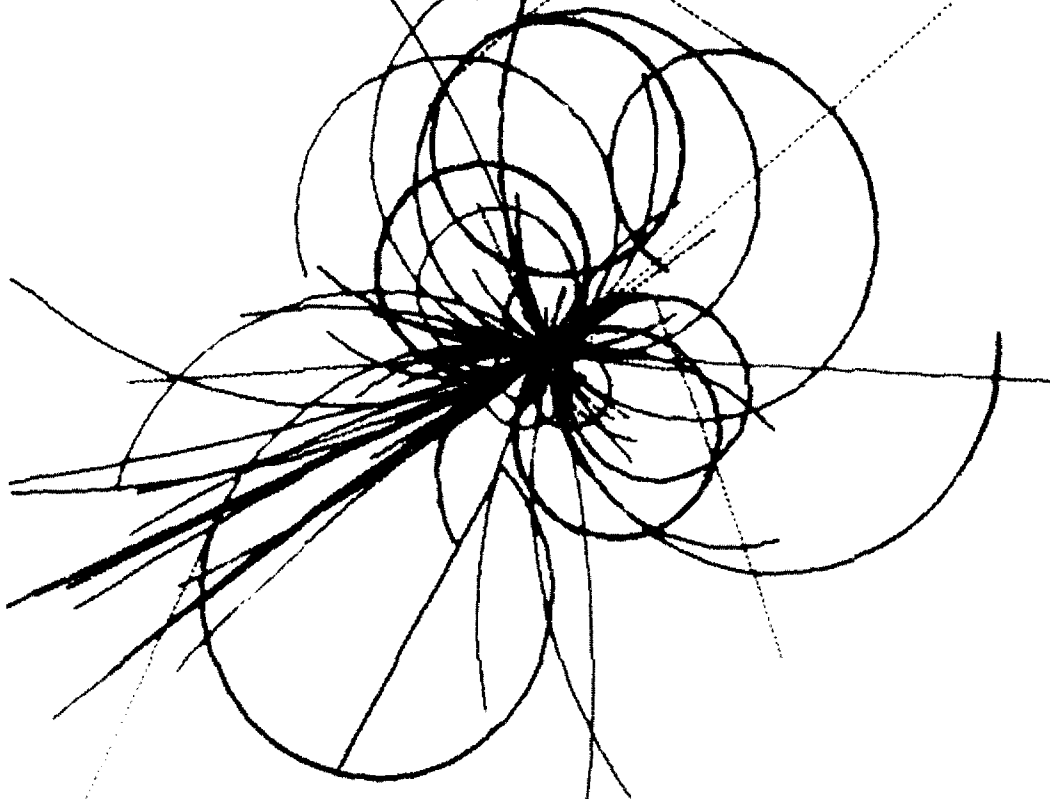


The Superconducting Super Collider



Radiation Levels in SSC Detectors

**Donald E. Groom
SSC Central Design Group**

August 3, 1988

RADIATION LEVELS IN SSC DETECTORS

Donald E. Groom,
for the Task Force on Radiation Levels
in the SSC Interaction Regions

SSC Central Design Group*
Lawrence Berkeley Laboratory 90-4040
Berkeley, California 94720

3 August 1988

This report is based upon talks given at the *International Conference on Advanced Technology and Particle Physics* (Como, Italy, 13–17 June 1988) and at the *1988 Summer Study on High Energy Physics in the 1990's* (Snowmass, Colorado, 27 June–15 July, 1988). It has been submitted to Nuclear Instruments and Methods for inclusion in an issue which will constitute the *Proceedings* of the Lake Como meeting. It is essentially a summary of SSC-SR-1033, the report of the Task Force on Radiation Levels in the SSC Interaction Regions. New material on the extension of the results to other hadron colliders is presented in Section 5.

* Operated by the Universities Research Association for the U. S. Department of Energy.

RADIATION LEVELS IN SSC DETECTORS

Donald E. GROOM, for the *Task Force on Radiation Levels in the SSC Interaction Regions**

SSC Central Design Group,[†] Lawrence Berkeley Laboratory 90-4040, Berkeley, California 94720, USA

Received _____

Estimates of ionizing dose and neutron fluence have been made for typical SSC detector configurations exposed to radiation from p-p collisions. Using standard descriptions of average events in conjunction with simulations of secondary processes, it is found that in most cases the radiation exposure can be parameterized by functions of the form $A \langle p_{\perp} \rangle^{\alpha} \cosh^{\alpha'} \eta$, where $\eta (= -\ln \tan \theta/2)$ is the pseudorapidity, the exponent α lies between 0.5 and 1.0, and $\alpha' = \alpha$ or $\alpha + 2$, depending upon the problem. A calorimeter element 2 m from interaction point and 6° from the beam line is subjected to an annual dose is 0.1 MGy at shower maximum. The annual neutron fluence in a central cavity of this radius exceeds 10^{12} cm^{-2} . The annual dose from the direct flux of charged particles scales inversely as the square of the distance from the beam line and is 0.4 MGy at 1 cm. A detector at an 8 TeV on 8 TeV p-p collider with the same "physics reach" would experience about 27 times as much radiation.

1. Introduction

High energy and high luminosity combine to create a radiation environment for experiments the Superconducting Supercollider (SSC) which is orders of magnitude more severe than at existing accelerators. Radiation problems must be addressed in any serious detector design. An SSC Central Design Group Task Force was therefore formed to make as quantitative an assessment of the radiation level as possible in the absence of a specific detector design. The Task Force Report is now available[1]. In the following we briefly summarize the approach and main results.

In an SSC interaction region (IR) most of the radiation comes from the 20 TeV on 20 TeV p-p collisions. At the design luminosity, about 10^8 collisions per second occur, and we assume that this luminosity is maintained for 10^7 s out of each year. At this luminosity the beam-beam collisions at each IR contribute

* F. S. Alsmiller, R. G. Alsmiller, Jr., S. Ban, J. E. Brau, K. W. Edwards, A. Fassò, H. Fesefeldt, T. A. Gabriel, M. G. D. Gilchriese (Chairman), D. E. Groom, H. Hirayama, H. Kowalski, H. W. Kraner, N. V. Mokhov, D. R. Nygren, F. E. Paige, J. Ranft, J. S. Russ, H. Schönbacher, T. Stanev, G. R. Stevenson, A. Van Ginneken, E. M. Wang, R. Wigmans, and T. P. Wilcox, Jr.

† Operated by the Universities Research Association for the U. S. Department of Energy.

$(300 \text{ hr})^{-1}$ to the reciprocal of the current lifetime, so collision products strike the detector at a rate which is equivalent to the accidental loss of one beam into the apparatus every 6 days. By comparison, beam-gas collisions and expected particle loss contribute very little. Accidental processes such as beam loss during injection are more problematical, but if they are significant severe machine damage will also result.

For purposes of this study, a detector has been modeled as a calorimeter surrounding an empty volume, with collisions occurring at the center. The calorimeter is a spherical shell extending to some cutoff angle from the beam line, typically 6° . More distant endcap calorimeters provide coverage from this angle to a smaller angle. Since results may be scaled with distance from the interaction point in a fairly simple way, the exact geometry is not critical. It is also not difficult to apply the results to specialized detectors currently being discussed, such as a forward B spectrometer in an intermediate-luminosity IR.

A incident hadron produces both an ionizing dose and a neutron fluence in a calorimeter. Backscattered neutrons enter the central cavity, and there might be substantial rear leakage from the calorimeter. About a third of the particles from the primary collision are π^0 's, so as many photons as hadrons strike the calorimeter. The resulting showers produce an ionizing dose which peaks more sharply and therefore more intensely than does the dose from an electromagnetic cascade. Backscattered photons re-enter the cavity.

A very simple approach has been used to describe all of these processes. In the first place, particle production is described—not particle production in the rare interactions of physics interest, but in the “minimum bias” events which occur 10^{15} times each year. Secondly, the interactions of single hadrons or photons with the detector are described and parameterized as a function of incident energy or momentum. The results are then combined to obtain the desired dose rate or flux. In a few cases “global” calculations have also been made; these corroborate the general approach but raise a few caveats. There are uncertainties in both particle production and in the effects of individual particles, and some of the assumptions are approximate. For example, the transverse size of a cascade is assumed to be small compared with distances over which the incident flux changes appreciably, an assumption which is certainly not valid very close to the beam line. Uncertainties from all of these sources are such that the results are thought to be dependable to within factors of two to four.

2. Particle production

Particle production at $\sqrt{s} = 40 \text{ TeV}$ has been studied with the aid of ISAJET[2], PYTHIA[3], and DTUJET[4]. In spite of some theoretical problems, a reasonable extrapolation from lower energies is possible because of the

relatively slow variation of the data with $\ln s$. The increasingly important cross section for producing low- p_{\perp} jets is included. For example, when ISAJET is used to generate a sample of “average” events, half MINBIAS and half TWOJET events are used. In all contexts, it is possible to write the charged multiplicity per average event as a function of pseudorapidity η (where $\eta \equiv -\ln \tan \theta/2$) and the component of momentum perpendicular to the beam direction in factored form:

$$\frac{d^2 N_{\text{charged}}}{d\eta dp_{\perp}} \approx H f(p_{\perp}) . \quad (1)$$

Equivalently,

$$\frac{d^2 N_{\text{charged}}}{d\Omega dp_{\perp}} \approx \frac{H f(p_{\perp})}{2\pi \sin^2 \theta} . \quad (2)$$

Here $f(p_{\perp})$ is a normalized function of p_{\perp} , and H , the height of the pseudorapidity plateau, is constant to within 10% or better for $|\eta| < 6$, corresponding to angles greater than 0.3° .

Several forms have been used for the function $f(p_{\perp})$. A form proportional to $p_{\perp} \exp(p_{\perp}/B)$ is usually sufficient, since the “skirt” appearing in the experimental distribution at high p_{\perp} has little effect in radiation calculations. For most applications the distribution given by Eq. 1 is folded with a single-particle response of the form Np^{α} , where $0.5 < \alpha < 1.0$. Integration results are changed by less than 10% if realistic forms for $f(p_{\perp})$ are replaced by

$$f(p_{\perp}) (= f(p/\sin \theta)) = \delta(p_{\perp} - \langle p_{\perp} \rangle) . \quad (3)$$

The best values for H and $\langle p_{\perp} \rangle$ are obtained by extrapolating experimental results. The central height of the rapidity plateau is shown in Fig. 1. With the exception of the circles indicating preliminary CDF data[5], the data points and fits are taken from Ref. 6. A reasonable extrapolation is to $H = 7.0$ at 40 TeV. Since the central value tends to be somewhat lower than the average, we have taken $H = 7.5$ as the average.

Similarly, $\langle p_{\perp} \rangle$ is shown in Fig. 2[5]. The extrapolation to 40 TeV is uncertain, but we have taken $\langle p_{\perp} \rangle = 0.60$ GeV/c for our present purposes.

About half as many π^0 's as charged hadrons are produced in the primary collision, with a distribution given by Eq. 1 except with a value for H which is half as large. We therefore assume the same number of (decay) photons per rapidity interval as charged particles, with a momentum distribution which has half the mean value as that for charged hadrons.

3. Effect of individual particles

Monte Carlo programs were used to simulate the results of a single photon or hadron striking a calorimeter. For incident hadrons, the dose and neutron flux inside, the neutron leakage from the back, and neutron backscatter from the front were calculated, although not always at the same time. EGS4[7] was used for electromagnetic simulations. Members of the Task Force variously used CASIM[8], FLUKA86[9], GHEISHA[10], HETC[11], and MARS10[12] for hadronic cascade simulations. With the exception of GHEISHA, these codes do not transport neutrons with energies below some cutoff, typically chosen as 50 MeV. For several problems in which these neutrons were important the codes ANISN[13], MORSE[14], and COG[15] were used.

In a few cases experimental data were also available. The associated errors were quite large because of interpretative problems. For example, a neutron flux might be measured using activation techniques, but with a reaction whose energy threshold was high compared with the energies of neutrons in the cascade. More and better experimental results are badly needed.

The calorimeters studied varied from uranium with silicon readout to iron with proportional wire chamber readout. As might be expected, neutron fluxes were highest for uranium with nonhydrogenous readout and lowest for iron with scintillator readout. A very rough comparison of neutron yield for several common configurations is shown in Table 1. The results should be used with caution at this stage, since (a) it was not possible to normalize all calculations to the same reference structure and (b) the scatter between different simulations was quite large. A systematic study of this problem would be quite useful.

The most commonly modeled calorimeter was a “fine-sampling uranium/scintillator calorimeter,” with alternating 3 mm uranium plates and 3 mm scintillator sheets. This was taken as a reference standard for the study.

A simple example of single-particle simulation results is shown in Fig. 3, in which the number of backscattered (albedo) photons above two energy thresholds is shown as a function of incident photon energy. There was no particular motivation for a power law fit in this and other cases, but it provided an adequate description. The yield cannot increase faster than linearly with E , and because higher energy showers peak deeper in the calorimeter a less than linear rise with energy is expected.

A more complicated case is shown in Fig. 4. The results from four simulations and two experiments (shown by the ellipses) are indicated by various letters. Hadronic cascades are more difficult to describe than electromagnetic showers, and the scatter indicates differences between codes. The solid line is drawn by

eye, and the dotted lines are the same curve shifted by factors of two. It is from these and similar data that we have concluded that our results for the response to single incident particles are probably valid to within factors of two.

As a hadronic cascade progresses, charged secondaries tend to “range out,” so that below a few tens of MeV the only hadrons of any significance are neutrons. One may think of a “gas” of such neutrons, diffusing away from the shower core, out of the front face of the calorimeter, and out the back. A sampling of calculated spectra for neutrons from the front face is shown in Fig. 5. According to this model, it is representative of the neutron spectrum inside the calorimeter, although one might expect a harder contribution near the shower core. The distribution in the logarithm of the kinetic energy is roughly gaussian, with a maximum at 1.3 MeV and a standard deviation corresponding to a factor of 3.7 from the mean, as shown by the smooth curve in Fig. 5. This “1 MeV” spectrum is characteristic of all processes we have examined. In some situations it is found to be slightly softer (e.g. the neutrons escaping from the Tevatron or SSC dipoles as a result of beam-gas losses) and in some slightly harder, but in general most of the neutrons under the peak are above the effective threshold for damaging silicon devices (about 0.15 MeV) and have a silicon damage coefficient close to that for 1 MeV neutrons.

In a few cases neutron transport was extended to thermal energies. The thermal flux is very close to the “1 MeV” flux, and we believe it has little importance in the present context.

A final consideration concerns the enhancement of the neutron flux in the central cavity due to further backscattering of neutrons from the calorimeter. The calculations indicate that the flux of in the cavity should be multiplied by about two to include this effect. The effect of holes in the detector near the beam line can be taken into account by multiplying the reflection probability by the fraction of the total solid angle subtended by the central calorimeter. In most practical cases this does not substantially change the answer.

4. Results

It follows from Eq. 2 that the flux of charged particles through a small counter with area da normal to the radius vector to the interaction point and at a distance r_{\perp} from the beam line is given by

$$\frac{dN_{\text{charged}}}{da} = \frac{1.2 \times 10^8 \text{ s}^{-1}}{r_{\perp}^2} \quad (4)$$

for r in cm and for the assumed interaction rate of 10^8 s^{-1} . In a light material $dE/dx \approx 1.8 \text{ MeV g}^{-1}\text{cm}^2$, so 1 Gy corresponds to 3×10^9 particles/cm². The

annual dose in a thin detector r_{\perp} from the beam line is then

$$D = \frac{0.4 \text{ MGy}}{r_{\perp}^2} \quad (5)$$

for r_{\perp} in cm and for assumed operation at design luminosity for 10^7 s per year.

As discussed in the previous section, the effect (dose, fluence, number of backscattered particles, etc.) could usually be parameterized by a power law in the incident momentum. For example, the radially integrated neutron fluence for one incident hadron on a uranium/scintillator calorimeter can be written as

$$\int \varphi da = N_n p^{\alpha} \quad (6)$$

with $N = 18$ and $\alpha = 0.67$, where p is measured in GeV/c ($p \approx E$) over most of the regions of interest). This integral is equal to the fluence at the same depth if one particle with momentum p is incident per unit area. The total response at that point may then be found by multiplying by the particle distribution (some variant of Eq. 1 or 2) and integrating over momentum. The integral may be carried out over all momenta, or over momenta above a cutoff imposed e.g. by a central solenoid. This has been done using a variety of forms for $f(p_{\perp})$. As discussed in Section 2, in the absence of a momentum cutoff accuracy well within the uncertainties in single-particle response is obtained with $f(p_{\perp}) = \delta(p_{\perp} - \langle p_{\perp} \rangle)$. It follows immediately that the response *per rapidity interval* per average p-p collision can be written in the form

$$H N \langle p_{\perp} \rangle^{\alpha} \cosh^{\alpha} \eta, \quad (7)$$

where the single-particle response is $N p^{\alpha}$ and where we have made use of the identity $\sin \theta \cosh \eta = 1$. Since $d\eta/d\Omega = 1/2\pi \sin^2 \theta$, the effect per unit solid angle, per unit area, or per unit mass is of the form $H N \langle p_{\perp} \rangle^{\alpha} \cosh^{\alpha+2} \eta$. In general,

$$\text{Dose or fluence} = A \langle p_{\perp} \rangle^{\alpha} \cosh^{\alpha'} \eta \quad (8)$$

where $\alpha' = \alpha$ or $\alpha + 2$, depending upon the problem. With few exceptions, all radiation fields in detectors may be written in this form.

The flux of particles incident on a detector at a given point scales inversely as the distance from the interaction point. Less obviously, the flux of backscattered neutrons and photons in the cavity defined by the calorimeter also scales inversely as the square of the linear dimensions. As a matter of convenience we have

standardized either to an inside radius of 2 m or to a distance of 2 m to the interaction point, but the scaling of all radiation effects with the inverse square of typical detector dimensions must be kept in mind. The penalties for a compact detector design are obvious.

We illustrate the approach with two examples. Fig. 6 shows the maximum annual neutron fluence in a uranium/scintillator calorimeter under standard operating conditions. Fig. 7 shows the annual ionizing dose produced by hadrons (solid curve) and photons (dashed curve) under the same conditions. Although photons carry only about half the energy as do the charged particles, the showers peak more sharply and thus have higher maxima. As might be expected, the dose ratio is about the ratio of a nuclear interaction length to a radiation length. A calorimeter is exposed to the highest radiation levels near the electromagnetic shower maximum.

A similar distribution for the number of backscattered neutrons per pseudo-rapidity interval may be integrated to find the neutron flux inside the cavity. For a uranium/scintillator calorimeter with a 2 m inner radius extending to within $|\eta| = 3$ (or 6°) of the beam line, the annual neutron fluence is given by

$$\Phi = 1.2 \times 10^{12} (1 + \text{reflection}) \text{ cm}^{-2} , \quad (9)$$

where “reflection” is mean number of subsequent reflections the neutron experiences before it loses substantial energy or is absorbed. Simulations of this problem indicate that $(1 + \text{reflection}) \approx 2$ for most calorimeters.

5. Application to other hadron colliders

In the context of the approximations summarized in Eqs. 7 and 8, the dose or fluence at any point in a detector at a hadron collider scales as

$$\text{Dose or fluence} \propto \left(\int_T \mathcal{L} dt \right) \sigma_{\text{inelastic}} H \langle p_{\perp} \rangle^{\alpha} . \quad (10)$$

For comparison purposes we assume the same duty cycle for all colliders and replace the luminosity integral by its nominal value. The factors appearing in Eq. 10 are evaluated in Table 2 for the Tevatron, the high-luminosity version of the proposed large hadron collider (LHC), and the SSC. The exponent α varies from 0.5 for neutron backscattering to 0.9 for the maximum electromagnetic and hadronic dose; for scaling purposes we take 0.9 as typical. An inelastic cross section of 100 mb has been adopted for 40 TeV[16]. This value has been crudely scaled with the aid of a fit to existing data to obtain the values given in the

Table.* The values of H and $\langle p_{\perp} \rangle$ are obtained from Figs. 1 and 2. The final row gives radiation scale factors, normalized to 1.0 for the SSC. The nominal luminosity given for the Tevatron is fairly arbitrary, but in any case most of the radiation experienced by detectors at the Tevatron collider comes from other sources, such as the main ring.

6. Conclusions

A combination of uncertainties about the inelastic cross section, multiplicity, and mean transverse momentum lead to uncertainties of perhaps two in our description of particle production at the SSC. Similar uncertainties exist in parameterizing single-particle response. In most cases, estimates of radiation levels in SSC detectors are therefore thought to be valid to within factors ranging from two to four. In certain restricted regions (e.g. very near the beam line) our approximations compromise the accuracy of the results.

Conclusions concerning the effect of this radiation on materials used in detectors are outside the scope of this study.[†] However, it appears likely that with sufficient care in the choice of materials radiation damage will not be the limiting factor in the lifetime of most parts of a large general-purpose detector at the SSC. This qualified statement could not be made if the design luminosity were an order of magnitude higher.

* There is recent evidence from cosmic ray measurements at high energies[17] and coulomb-nuclear interference measurements at the S \bar{p} pS[18] that the inelastic cross section at 40 TeV may be substantially larger than 100 mb, perhaps by as much as 50%[19]. We will await Tevatron results before revising any conclusions.

[†] However, see Refs. 20 and 21. Further studies are in progress, particularly concerning the availability of radiation-hard electronics technology.

Table 1

Relative maximum neutron flux and backscattered neutron flux for various calorimeter configurations.

Calorimeter	Relative flux
U-LiqAr or Si	1.0
Pb-LiqAr or Si	0.5
U-Scint.	0.3
Pb-Scint.	0.15

Table 2

A rough comparison of beam-collision induced radiation levels at the Tevatron, SSC, and high-luminosity LHC.

	Tevatron	LHC	SSC
\sqrt{s} (TeV)	1.8	16	40
\mathcal{L}_{nom} ($\text{cm}^{-2}\text{s}^{-1}$)	5×10^{29}	4×10^{34}	1×10^{33}
$\sigma_{\text{inelastic}}$	59 mb	86 mb	100 mb
H	4.1	6.3	7.5
$\langle p_{\perp} \rangle$ (GeV/c)	0.46	0.55	0.60
Scale factor	1.3×10^{-4}	27	1

References

- [1] Report of the Task Force on Radiation Levels in the SSC Interaction Regions, SSC Central Design Group Report SSC-SR-1033 (June 1988).
- [2] F. E. Paige and S. D. Protopopescu, "ISAJET 5.35, A Monte Carlo Event Generator for p-p and p- \bar{p} Reactions," ISAJET PAM file; F. E. Paige and S. D. Protopopescu, in *Physics of the Superconducting Supercollider*, ed. by R. Donaldson and J. Marx (Snowmass CO, 1986) p. 320.
- [3] H.-U. Bengtsson, Torbjörn Sjöstrand, "The Lund Monte Carlo for Hadronic Processes- PYTHIA version 4.8," LU TP 87-3 (Jan 1987); H. U. Bengtsson and T. Sjöstrand, in *Physics of the Superconducting Supercollider*, ed. by R. Donaldson and J. Marx (Snowmass CO, 1986) p. 311.
- [4] J. Ranft, P. Aurenche, F. Bopp, A. Capella, K. Hahn, J. Kwiecinski, P. Maire and J. Tran Thanh Van, SSC Central Design Group Report SSC-149 (1987).
- [5] S. Errede and A. Para, private communications (May 1988).
- [6] G. J. Alner *et al.* (UA5), Z. Phys. C **33** (1986) 1-6.
- [7] W. R. Nelson, H. Hirayama and D. W. O. Rogers, "The EGS4 Code System," SLAC-265, Stanford Linear Accelerator Center (Dec. 1985).
- [8] A. Van Ginneken, Fermilab Report FN-272, Fermilab, Batavia, IL, USA (1975).
- [9] P. A. Aarnio, A. Fassò, H.-J. Möhring, J. Ranft and G. R. Stevenson, CERN TIS-RP/168 (1986).
- [10] H. Fesefeldt, "The Physics of Hadronic Showers—Physics and Applications," RWTH Aachen PITHA 85/02 (1985).
- [11] R. G. Alsmiller, Jr. *et al.*, "Modifications of the High Energy Transport Code (HETC) and Comparisons with Experimental Results," presented at the ANS Topical Conference on Theory and Practices in Radiation Protection and Shielding, 22-24 April 1987, Knoxville, Tennessee; K. C. Chandler and T. W. Armstrong, "Operating Instructions for the High-Energy Nucleon-Meson Transport Code HETC," Oak Ridge National Laboratory Report ORNL-4744 (1972)
- [12] N. V. Mokhov, IHEP Preprint 82-168, Serpukov, USSR (1982); A. N. Kalinovsky, N. V. Mokhov and Yu. P. Nikitin, Penetration of High Energy Particles through Matter, (Energoatomizdat, Moscow, USSR) (1984).
- [13] W. W. Engle, Jr., "A User's Manual for ANISN, A One-Dimensional Discrete Ordinates Transport Code with Anisotropic Scattering," K-1693, Union Carbide Corporation, Oak Ridge, TN (1967).

- [14] M. B. Emmett, "The MORSE Monte Carlo Radiation Transport Code System," Oak Ridge National Laboratory Report ORNL-4972 (February 1975).
- [15] T. P. Wilcox, Jr., E. M. Lent, "COG: A Particle Transport Code Designed to Solve the Boltzman Equation for Deep-Penetration (Shielding) Problems—Volume I, Users Manual," Lawrence Livermore National Laboratory Report M-221-1.
- [16] D. E. Groom, "The Total p-p Cross Section at 40 TeV," SSC Central Design Group Note SSC-N-154 (1986).
- [17] T. K. Gaisser, U. P. Sukhatme, and G. B. Yodh, *Phys. Rev.* **D36** (1987) 1350.
- [18] UA4 Collaboration, *Phys. Lett.* **B198** (1988) 583.
- [19] M. Block, *Proc. of the 1988 Summer Study on High Energy Physics in the 1990's*, (Snowmass, Colorado) (to be published).
- [20] Report of the Task Force on Radiation Effects at the SSC, SSC Central Design Group Report SSC-SR-1035 (1988).
- [21] H. Schönbacher and A. Stolarz-Iżycka, "Compilation of Radiation Test Data, Part I: Cable Insulating Materials," CERN Report CERN79-04 (1979); H. Schönbacher and A. Stolarz-Iżycka, "Part II: Thermosetting and Thermoplastic Resins," CERN 79-08 (1979); P. Beynel, P. Meyer, and H. Schönbacher, CERN 82-10 (1982).

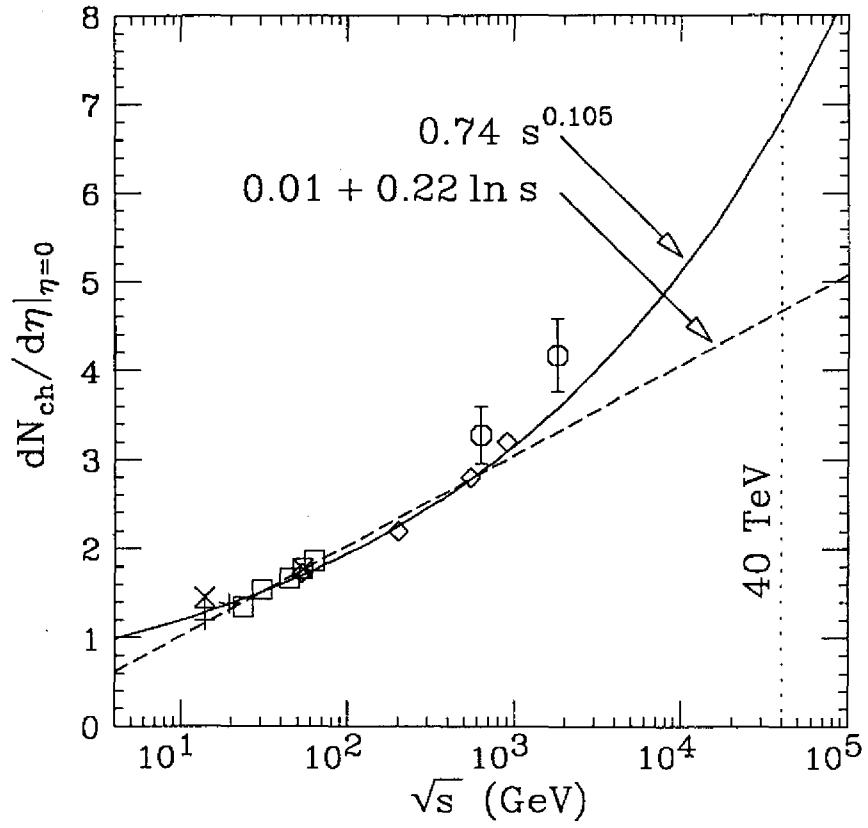


FIG. 1. $dN_{\text{charged}}/d\eta|_{\eta=0}$, based on FNAL fixed target (+ and ×), ISR (□), SppS (◇), and CDF (○) data. The preliminary CDF points[5] have been added to data taken from Fig. 2 in Alner *et al.* [6], and the two fits shown are to the data exclusive of CDF.

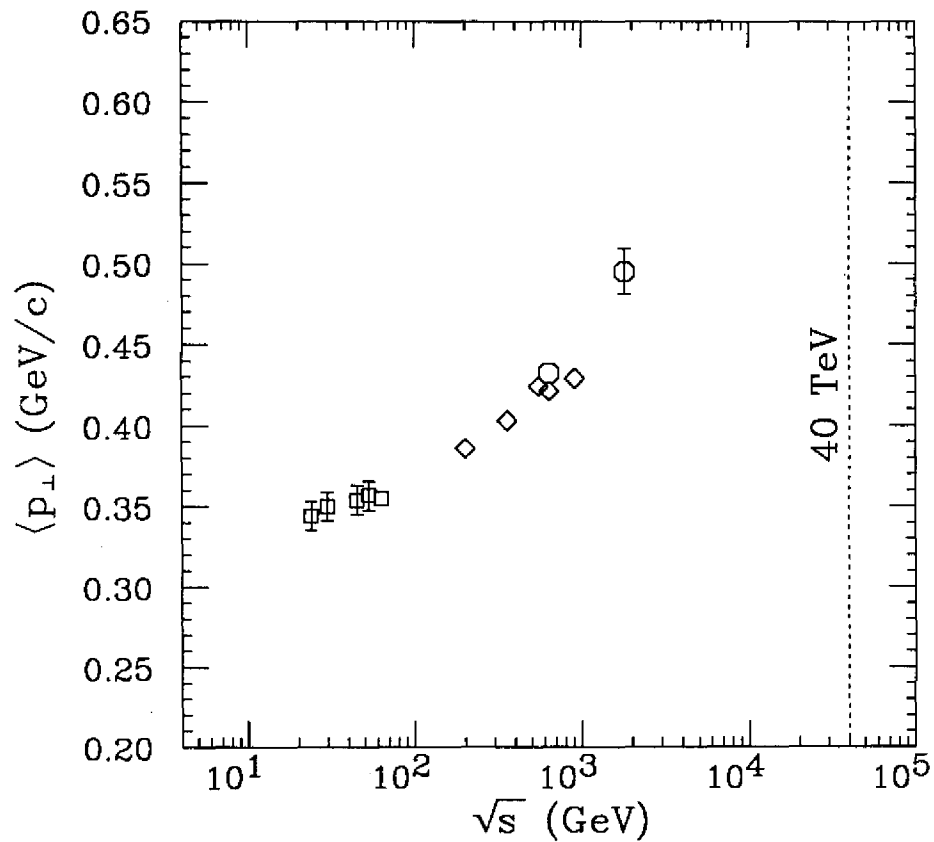


FIG. 2. The mean value of p_{\perp} for the distribution $d^2N_{\text{charged}}/dy dp_{\perp}$ as a function of center of mass energy for minimum bias events[5]. ISR (\square), SppS (\diamond), and preliminary CDF (\circ) results are shown.

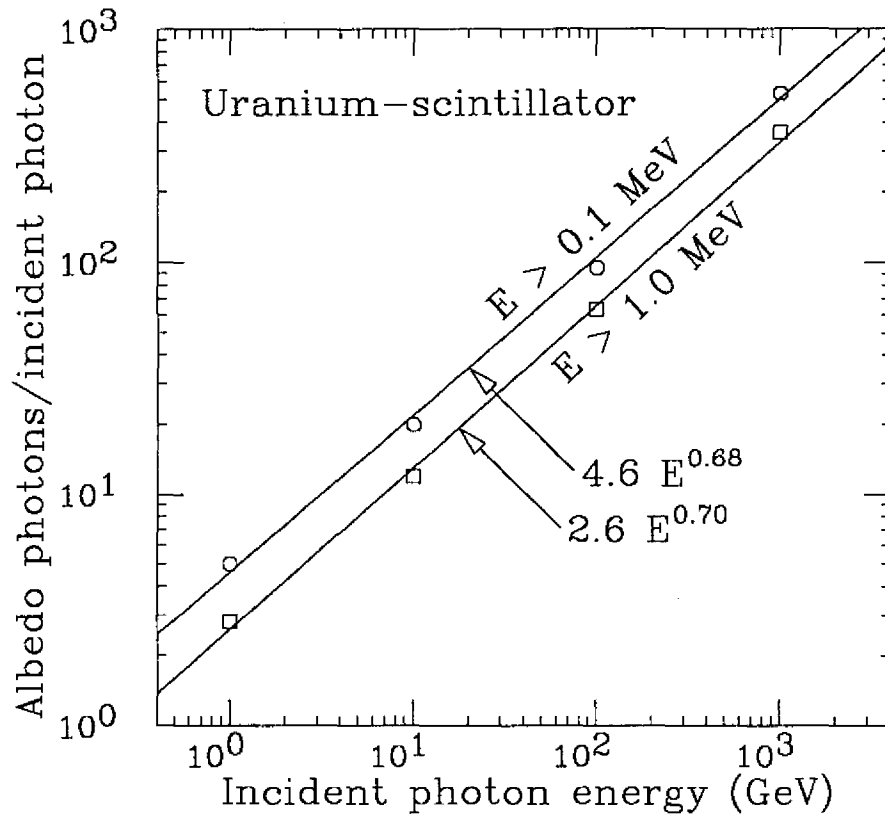


FIG. 3. The number of albedo photons for two different lower limits on the albedo photon energy vs. incident photon energy.

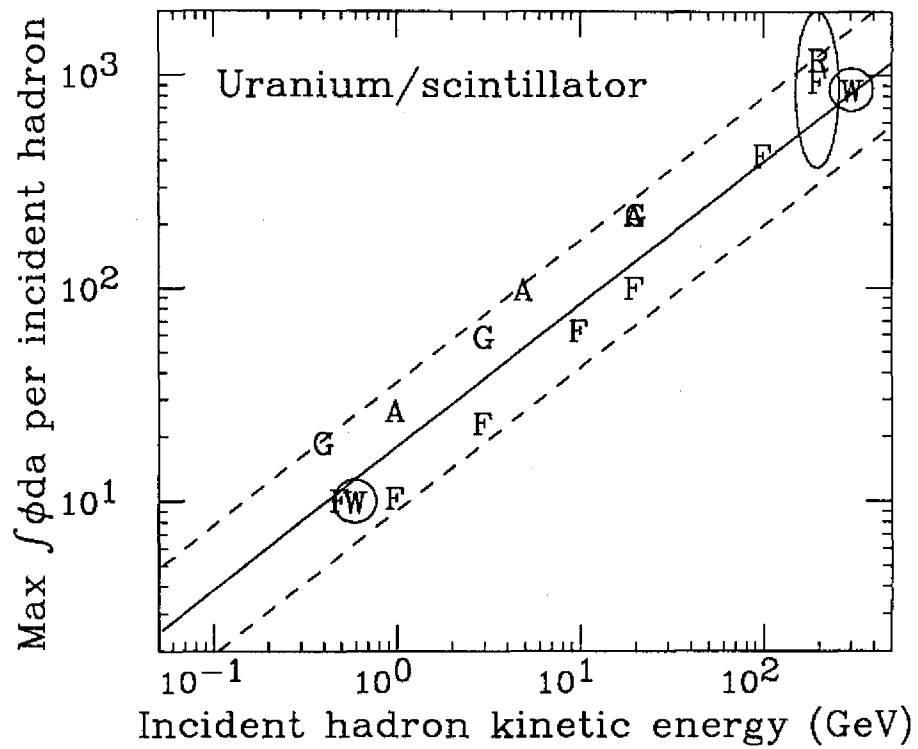


FIG. 4. Summary of selected maximum neutron flux data for a fine-sampling uranium/scintillator calorimeter. The solid curve represents $\int \phi da = 18 (E_k / (1 \text{ GeV}))^{0.67}$, while the dashed curves are higher and lower by a factor of two. E_k may be replaced by p for practical calculations.

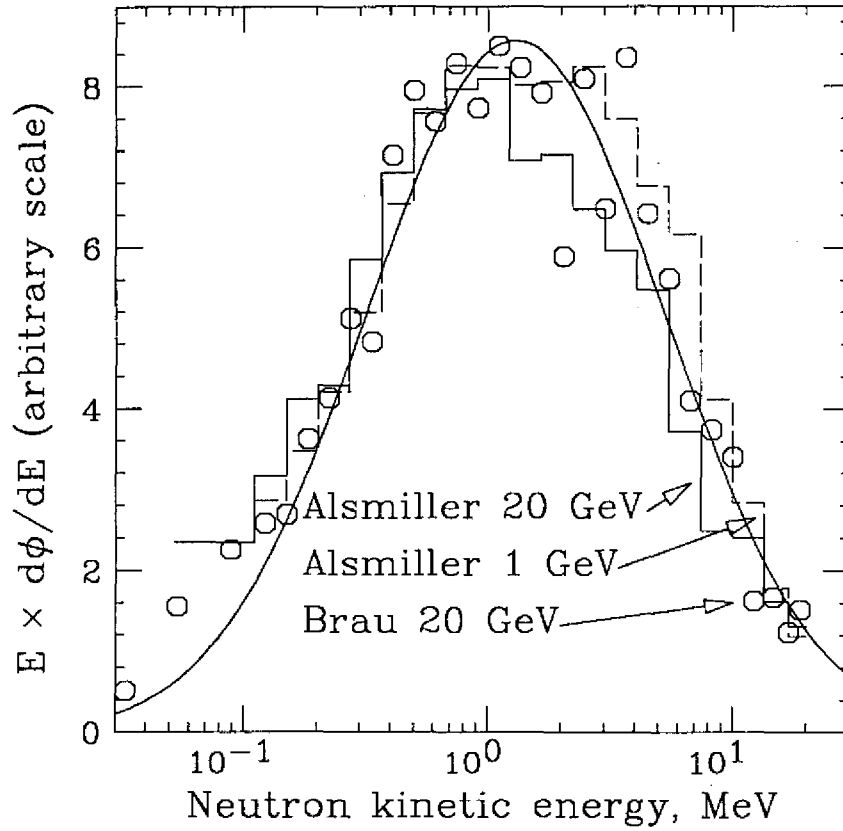


FIG. 5. The spectrum of neutrons backscattered from a uranium/scintillator calorimeter. The spectra at 1 GeV and 20 GeV were calculated by Alsmiller *et al.* (dashed and solid histograms), and a 20 GeV spectrum calculated by Brau and Gabriel is shown by the circles. Normalizations are chosen so that the peaks coincide. The solid curve is a gaussian in $\ln E_k$.

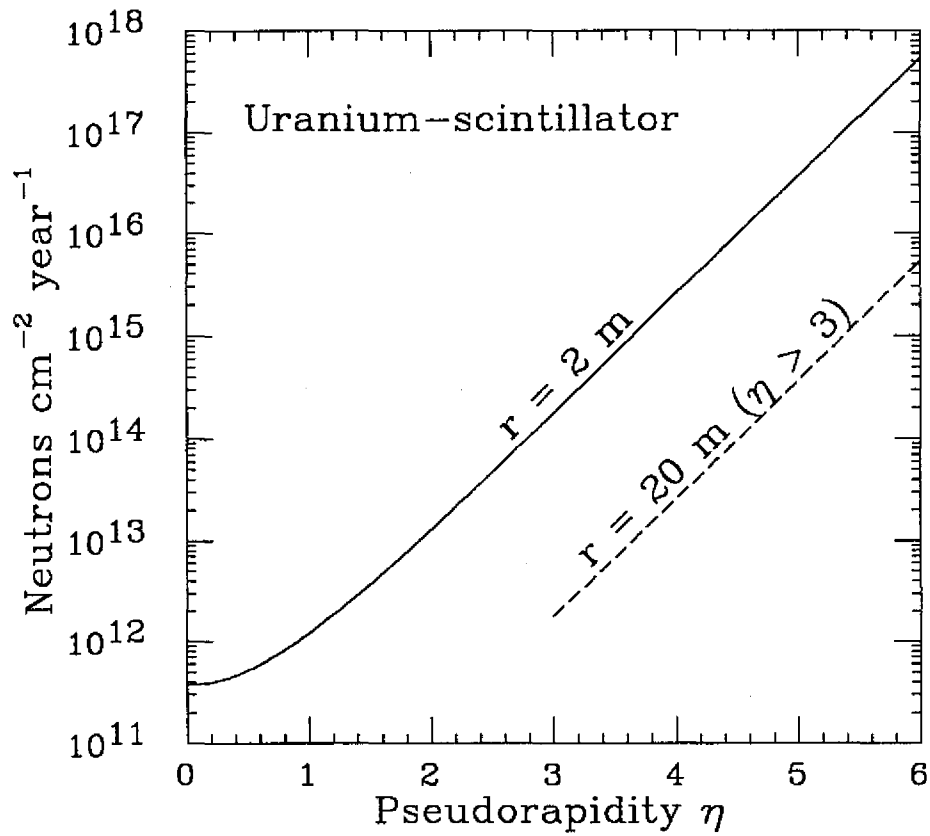


FIG. 6. The maximum neutron flux for a uranium/scintillator calorimeter. The solid curve shows the result assuming the maximum occurs at a radius of 200 cm. Also shown is the result for a radius of 20 m, typical of forward detectors, for rapidity > 3 .

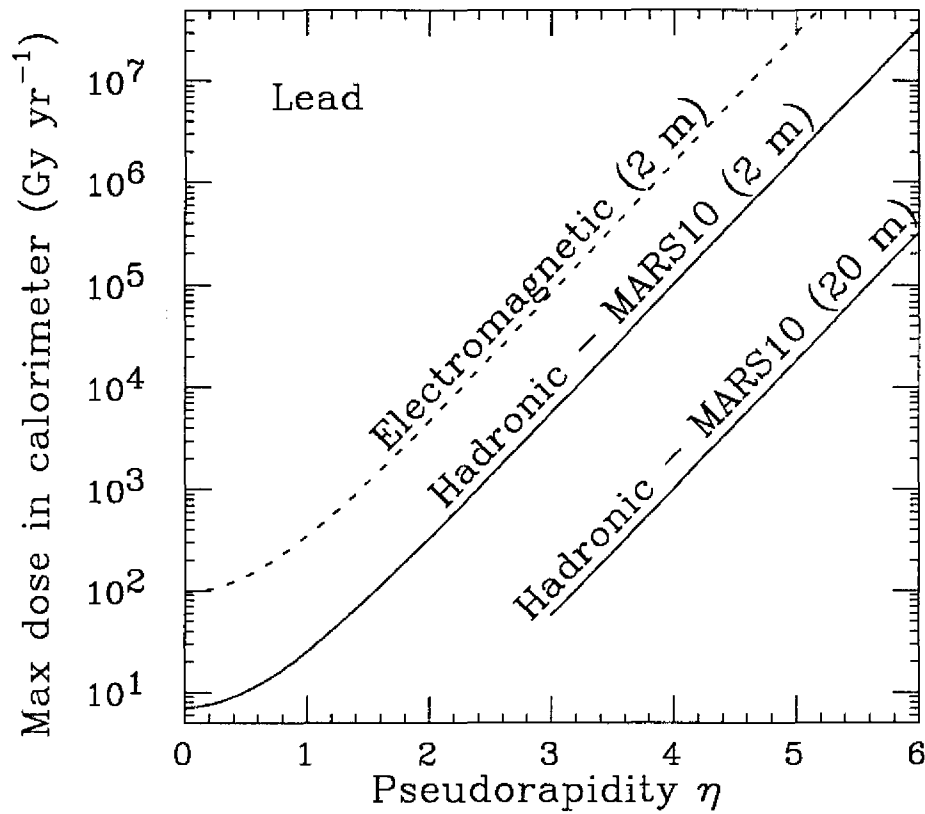


FIG. 7. The maximum hadronic dose as a function of pseudorapidity for a lead sphere, assuming that the maximum dose occurs at the indicated radius. The maximum electromagnetic dose in uranium/scintillator is shown by the dashed line. Since the radiation length, nuclear interaction length, and density are nearly identical for the two materials, dose (but not neutron flux) results may be compared directly.